lubricants

MDPI

Article

Influence of Copper/Graphite Properties on the Tribological and Electrical Behavior of Copper-Graphite Third Body Layer

Eric Chapteuil [1,*], Mathieu Renouf [2,3], Chaoqun Zeng [2] and Yves Berthier [1,3]

1 LaMCoS, Université de Lyon, INSA-Lyon, 69621 Villeurbanne, France; yves.berthier@insa-lyon.fr
2 LMGC, Université de Montpellier, CNRS, 34000 Montpellier, France; mathieu.renouf@umontpellier.fr (M.R.); chaoqun.zeng@univ-montp2.fr (C.Z.)
3 InTriG, 69621 Villeurbanne, France
* Correspondence: eric.chapteuil@insa-lyon.fr

Received: 11 October 2018; Accepted: 10 December 2018; Published: 14 December 2018

Abstract: The understanding of rail braking is irrevocably dependent on the tribological analysis of contacts such as the wheel/rail contact or the wheel/brake disc contact. Because it is very complex to experimentally analyze the inside of a contact, a numerical approach based on discrete element modeling was used to model a third body composed of copper and graphite, the main elements present in sintered brake materials. Simulations were analyzed by measuring several global quantities as a function of the proportion of copper and the local properties of the material to determine the extent to which local parameters influence the electrical and tribological properties of the third body. Among the results noted was the fact that a certain proportion of mixture makes it possible to achieve a balance between electrical and tribological properties.

Keywords: DEM; mixture; tribology; brake pad

1. Introduction

Improving high-speed trains requires a better control and understanding of the friction materials used in brake pads. Among the different kinds of materials (ceramic, metallic, etc.), copper-based materials are probably the most widely used in braking systems due to their good mechanical, electrical and tribological properties. In such a composite, the different components play a distinct role. The copper (Cu) matrix has good wear resistance and excellent thermal conductivity, but without specific treatment, its tribological performance is poor (surface scratches without lubrication). To overcome this tribological misbehavior, copper-based friction materials are combined with graphite (Gr), which has better tribological properties. As a result, copper/graphite (Cu/Gr) composites have a low coefficient of friction and low wear rates. The literature offers many works dedicated to the study of their properties, such as the surface condition of composites [1], their structural characteristics [2], the size of graphite particles, and the graphite concentration [3,4] on the measured global friction. However, the resulting friction is not only a material property but also depends on the contact conditions (environmental velocity pressure) [5], the mechanism that keeps the bodies in contact and the interface separating them, mainly composed of debris from the materials in contact, mixed with external elements. This interface, known as the third body [6], plays an important role in the evolution of friction. It plays a role in the separation of contact bodies, in the transmission of normal load and in the accommodation of speed [7]. In addition, the composition of the third body can significantly modify the tribological properties of Cu/Gr composites, as illustrated by numerous research studies [8–13].

Although several results make it possible to estimate the influence of the third body on the tribological properties of Cu/Gr composites, they highlight that it remains complex and difficult to control due to its strong correlation with the internal properties of the materials and contact conditions. Recent works attempt to highlight the interaction of the two main components of Cu/Gr composites as well as the contributions of each component to tribological properties (friction, wear, and electrical conductance) [8]. However, even if the friction dependence on the Cu/Gr ratio has been demonstrated, the range of shear velocities used remains limited to extend the results to applications involving Cu/Gr composites subjected to lower or higher speeds. In addition, measurements of the friction factor include both the rheology of the third body and the dynamic behavior of the structure (vibration and structural damping); the in situ life of the third body layer is still a mystery because it remains difficult to determine which parts between volume and surface properties influence the macroscopic measurements. These difficulties are inherent in in situ experiments. Since contact is confined, it is almost impossible to experimentally analyze phenomena occurring in the third body without disturbing experimental measurements. Moreover, post-mortem surface analysis does not allow to analyze the entire dynamic process, and only offers a final surface state and not the complete history of a contact's life.

To overcome this lack of information, numerical simulations appear to be a good compromise to complete the experimental observations, not to replace them. By controlling the different physical parameters of the simulations, it is then possible to carry out a more systematic parametric study of the contact. It also becomes possible to decouple the effects of the first and third bodies to extend or correct the experimental results [14]. Among the different numerical frameworks, a discrete element approach [15] was chosen to represent the rheology of the third body, in which several developments [16,17] allow simulating the multi-physical behavior of discontinuous and heterogeneous interfaces. Based on such a framework, this work studied the third body layer made of Cu/Gr composites, with a view to enriching knowledge on their rheology. The impact of global parameters such as the shear rate were studied, as well as local parameters such as Cu/Gr interactions, controlled by cohesion and friction parameters. Thus, after a presentation of the main lines of the numerical method used, the results of the digital surveys are discussed. Measurements of electrical resistance, porosity and friction are related to the composition of the layer (component ratio, friction, and cohesion) and compared to experimental results from the literature.

2. A Discontinuous Multi-Physical Framework

Due to its heterogeneity and discontinuity, modeling the third body layer is not an easy task. The identification and definition of a particle of a third body is still an open question today [18], which does not allow us to define a global behavior. As a result, classical modeling tools, derived from the mechanics of continuous media, are falling apart and alternatives must be found. Since the early work of Elrod and Brewe [19], discrete element methods (DEM) have emerged as a good way to be more representative of a third body layer [20]. However, this first kind of approach is based on an analogy between numerical and real particles, such as what is done at a more macroscopic scale to model granular media [21,22]. However, following the previous remark concerning the definition of a third body particle, the same questions can then be asked for a numerical particle: Should it be considered rigid or deformable, in which case with which behavior law? Should it be considered as circular or with a more complex geometry, but without deformation? What is the impact of geometry on the global behavior?

Following these many questions, without any real answer yet today, the DEM philosophy is used not to associate a digital particle with a real one but to make an analogy between a set of digital particles and an elementary volume of a third body layer. In this spirit, a digital particle represents the smallest element of matter that is considered undeformable. A volume of particles can thus be deformed according to the laws of interaction between elements and the latter can then be analyzed

from a mechanical point of view, but also from a thermal [23], electrical [16] or physico-chemical [24] point of view thanks to the various improvements in DEM methods.

Among the different DEM approaches available in the literature, the NSCD approach (Non-Smooth Contact Dynamics), introduced by Moreau and Jean [25], was used in this work. It is based on an implicit integration of the dynamic equation, coupled with a non-linear Gauss–Seidel resolution algorithm to solve the multi-contact problem, allowing the use of many interaction laws. The reader can refer to the original works for more details on the method [25]. In this numerical framework, a set of rigid circular particles is used to represent the third body layer. Interactions between elements are described by laws of cohesive unilateral contact, coupled with a Coulomb friction model [24]:

$$\begin{cases} r_n + \gamma \geq 0 \quad g \geq 0 \quad g(r_n + \gamma) = 0 \\ \|r_t\| \leq \mu r_n \end{cases}, \quad if\ g \leq d_w, \tag{1}$$

where r_n and r_t are the normal and tangential forces, g is the contact distance, μ is the local friction coefficient, γ is the cohesion force and d_w is the attraction distance. The complementarity problem corresponding to the first equation of the system is as follows. If the distance g is greater than the attraction distance, then there is no contact and r_n is zero. If g is between 0 and d_w, the particles only interact through the cohesive force. In this case, $r_n = -\gamma$ and $g > 0$. When there is contact, i.e., $g = 0$, $r_n \in [-\gamma, +\infty]$. In both cases, the product $(r_n + \gamma)g = 0$.

With such a local interaction law, similar to the Maugis–Dugdale model [26], it is possible to confer compressive strength to the layer and thus transfer the normal load from one body to another (represented here by two rigid, rough and non-deformable walls). The friction-related part ensures shear strength. The cohesive part of the law keeps particles connected when they are close enough. This model remains a simplified version of reality but it remains sufficiently representative to propose qualitative results [14].

To account for the electrical effects in such a discrete model, different assumptions are made. The first consists in assimilating the interaction network to a network of electrical resistances. The particles represent the nodes of the network while the interactions represent the different branches; each branch has its own electrical conductivity, depending on the properties of the connected particles but also on the intensity of the contact force. On the basis of such a network, the second hypothesis consists in building the electrical problem from the laws of Ohm and Kirshoff and solving it with an iterative algorithm such as a Gauss–Seidel algorithm [16] or a conjugated gradient [17,27].

The key point of the electrical model is based on the definition of local conductivity. Several local models are available in the literature [16,28]. The used model is based on the definition proposed by Zeng [17]. For each contact, the electrical current I is given by Ohm's law:

$$I = \Delta U / R, \tag{2}$$

where R represents the electrical contact resistance, which is determined by the classical model of electrical contact constriction proposed by Holm:

$$R = \rho / 2a, \tag{3}$$

where ρ denotes the electrical resistivity of the material and a is the radius of the effective contact surface. Such an equation is generally valid when $a <<< r$ (r being the radius of the particle) and the deformation of the particle remains low, which is the case with regard to the contact law used.

However, for small particles under high stress (which is the case in lubrication in the presence of a third body), the contact area is more likely to deform plastically than elastically. Therefore, it is more relevant to calculate the apparent contact area a, using the formula proposed by Bowden et al. [29]:

$$a = \sqrt{(r_n + \gamma) / \pi Y}, \tag{4}$$

where r_n is the contact force and Y is the yield strength. This equation is valid for the apparent contact surface; the real contact surface that allows the passage of electric current being smaller [30].

Thus, at the local level, the equivalent conductance (the inverse of the resistance) between two particles is calculated by taking into account the specific conductances of each particle as well as the mechanical conductance related to the contact force. It is expressed as:

$$C_\alpha = C_i C_j / (C_i + C_j + C_i C_j / C_m) \quad (5)$$

where i and j are the indices of the particles in contact and C_m is the mechanical conductance. If one of the conductances is zero, C_α =0 (in the case of insulating particles or when contact is lost).

3. Numerical Investigations

3.1. Model

To analyze the mechanical-electrical behavior of a sheared third body layer, an elementary shear cell is used. It is composed of a set of rigid circular particles representing the third body layer and two clusters of particles to delimit the system in the direction perpendicular to the shear direction. These two walls, rough and non-deformable, represent the first upper and lower bodies. A normal force is applied to the upper wall, while a speed is given to the lower one. Periodic conditions are applied in the shear direction to represent an infinite contact (cf. Figure 1).

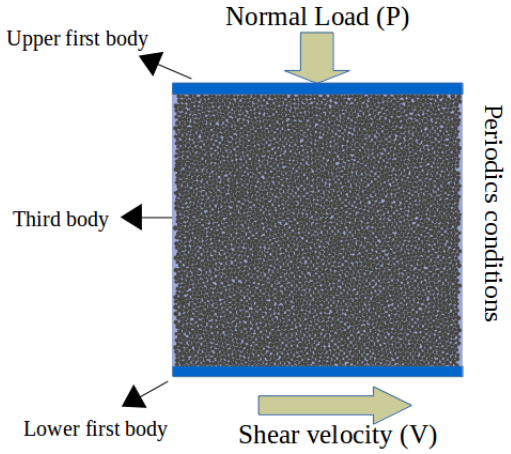

Figure 1. Numerical model.

In the following part of this work, different parametric studies using the parameters summarized in Table 1 are presented.

Table 1. Simulation parameters.

Material	Graphite	Copper
density (kg·m^{-3})	2.1×10^3	8.9×10^3
electrical conductivity (S·m^{-1})	3×10^5	5.9×10^7
internal friction	0.05	0.6
internal cohesion (N)	0.1	10
Particle number	4529	
Cell dimension ((m) × (m))	$(2 \times 10^{-2}) \times (2 \times 10^{-2})$	
Mean particle radius (m)	10^{-4}	
Pressure (MPa)	5×10^{-2}	

As mentioned in the Introduction, the current model was intended to be qualitative, not quantitative. The range of local parameters is wide enough to be consistent with the literature and to propose more general trends.

In addition, during shear, the evolution of different macroscopic quantities was analyzed. The first concerns the overall electrical resistance of the sample defined as the ratio between the electrical potential differential between the walls and the intensity of the current flowing through the medium (i.e., $R = U/I$). The macroscopic friction coefficient $\bar{\mu}$ was defined as the ratio between tangential forces and normal forces. Finally, the evolution of the dynamic and static porosity ratios [17,31], denoted Φ^*, was measured to follow the evolution of the internal texture of the sample.

3.2. Dry Frictional Mixture

First, non-cohesive mixtures were considered. Only friction effects were taken into account. The local friction of Gr/Gr and Cu/Cu were 0.05 and 0.6, respectively. Three Cu/Gr friction values were tested (0, 0.05 and 0.15) for different shear rates (0.2, 2 and 20 m/s).

Figure 2 presents the evolution of the global electrical resistance R as a function of the percent of Copper.

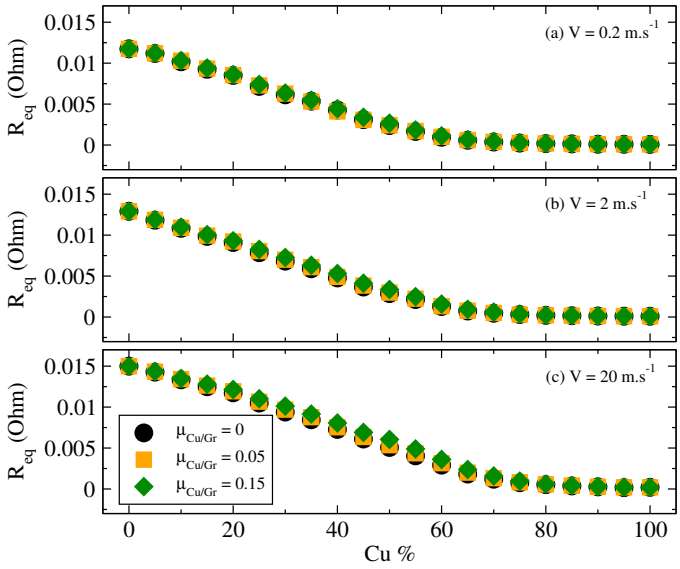

Figure 2. Evolution of the global electrical resistance for different Cu/Gr frictions (0, 0.05 and 0.15) and for different shear velocities: (**a**) 0.2 m/s; (**b**) 2 m/s; and (**c**) 20 m/s.

The electrical resistance R decreased with increasing copper proportion, from 10^{-2} Ohm (for 0% Cu) to 10^{-4} Ohm (for 100% Cu), i.e., two orders of magnitude of difference corresponding to the difference in conductivity of the two materials (see Table 1). The decrease of R was independent of the Cu/Gr friction value. Moreover, the decrease in electrical resistance was decomposed into two parts: a linear part between 0% copper and a percentage that seems to depend on the shear rate (close to 60% for 0.2 m/s and 80% for 20 m/s) and a constant part where the variations of R were not significant compared to the value at 0% copper. It can also be noted that the shear rate affected the transition point between the two phases and also resulted in an increase of R in the linear phase.

With respect to Figure 3, it is difficult to directly correlate the decrease in the global electrical resistance to the evolution of the variation of the porosity.

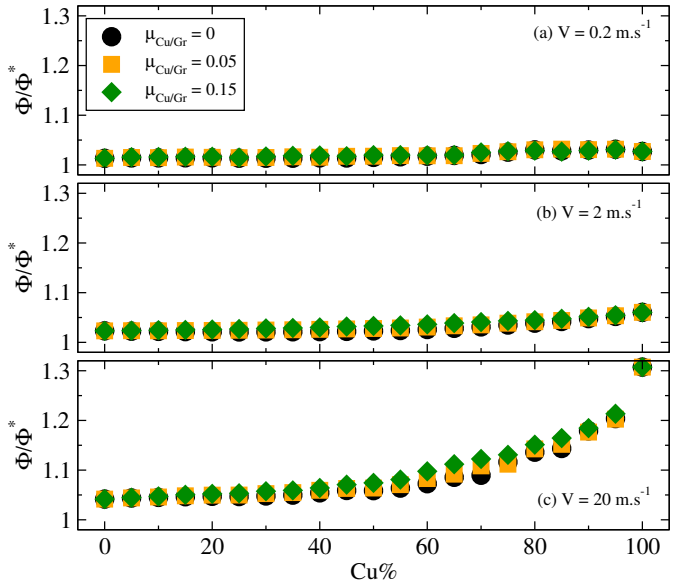

Figure 3. Evolution of the porosity variation for different Cu/Gr frictions (0, 0.05 and 0.15) and for different shear velocities: (**a**) 0.2 m/s; (**b**) 2 m/s; and (**c**) 20 m/s.

The evolution of Φ/Φ^* did not allow distinguishing the two phases observed previously. It was almost constant for velocities equal to 0.2 and 2 m/s. For the highest shear rate (i.e., 20 m/s), an increase of Φ/Φ^* was observed. This increase was more pronounced for mixtures composed of more than 50% of copper. However, this increase of porosity did not impact the global electrical resistance. Finally, as observed for the last one, the evolution of Φ/Φ^* was almost independent of the Cu/Gr friction value, and this for the different shear rates.

Finally, the evolution of the macroscopic friction coefficient $\bar{\mu}$ for different Cu/Gr friction was observed (cf. Figure 4).

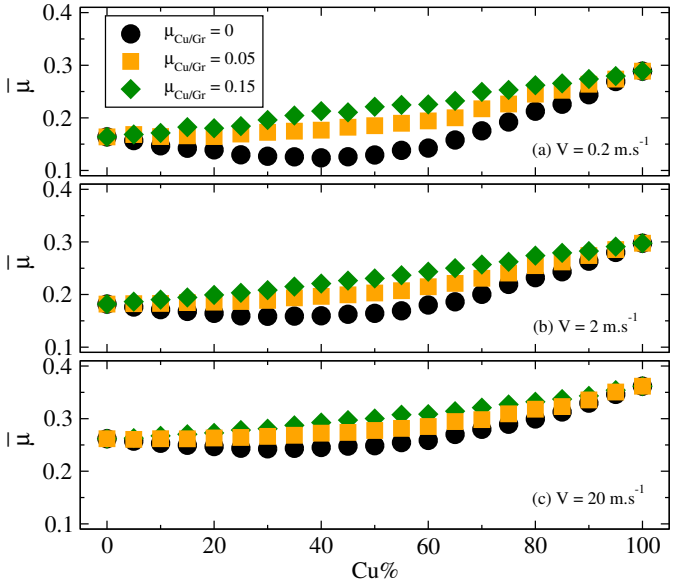

Figure 4. Evolution of the macroscopic friction coefficient for different Cu/Gr frictions (0, 0.05 and 0.15) and for different shear velocities: (**a**) 0.2 m/s; (**b**) 2 m/s; and (**c**) 20 m/s.

Compared to previous global measurements, local friction has a greater impact on the evolution of $\bar{\mu}$. When the Cu/Gr friction was equal to the Gr/Gr friction, $\bar{\mu}$ had a linear evolution, varying from 0.16 to 0.3. Then, when the Cu/Gr friction decreased, a loss of linearity was observed with a non-monotonic evolution for a zero friction value for a minimum close to 40% of copper. This trend was

not affected by the different shear rate values. Nevertheless, in the absence of local friction, the position of the minimum value of $\bar{\mu}$ changed and tended towards a copper percentage of approximately 30% (for a shear rate of 20 m/s). Finally, it can be noted that the increase in shear rate reduced the gap between the different curves.

Finally, for a given proportion of copper, the shear rate increased the overall values by $\bar{\mu}$, which is consistent with some results in the literature [8]. In view of the results presented above, mixtures with zero friction between the two components (i.e., Cu/Gr friction) were more sensitive than other mixtures. Such results reflect some experimental observations made in Linlin Su et al. [8,10], highlighting the importance of copper/graphite interaction on the overall behavior of the environment and the bodies in contact.

3.3. Cohesive Frictionless Mixture

If local friction were an important parameter, it was not of the first order on the evolution of macroscopic friction resulting from the shearing of a divided medium; the increase in local friction led to a saturation of macroscopic friction around a value close to 0.4 [32]. The use of local cohesive force allowed more important values to be measured [33]. Thus, after a study with dry mixtures (i.e., in the absence of cohesive forces), mixtures with only cohesive forces were studied.

To carry out these investigations, the value of local cohesion for Gr/Gr and Cu/Cu was set at 0.01 and 10 N, respectively, to respect the ratio between the values from the literature [8,9]. Three Cu/Gr cohesion values were used: 1, 10 and 50 N. The first value corresponded to an intermediate value between the Gr/Gr and Cu/Cu cohesion values. The second value was equal to the Cu/Cu cohesion, while the last value was taken as five times greater than the Cu/Cu cohesion to be able to extrapolate the results. As in previous analyses, the same range of shear rates was tested (i.e., 0.2, 2 and 20 m/s).

The overall electrical resistance showed a similar evolution to that of dry media (cf. Figure 5): a linear part decreasing with the increase of copper and an almost constant part for values above 60% of copper. The main difference was observed for the highest shear rate and the highest cohesion value. This case shows resistance variations occurring during linear decrease.

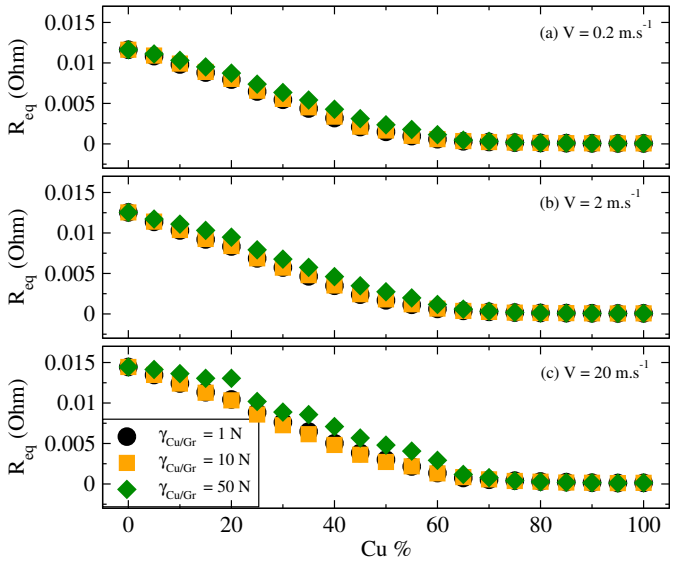

Figure 5. Evolution of the global electrical resistance for different Cu/Gr cohesion (1, 10 and 50 N) and for: (**a**) 0.2 m/s; (**b**) 2 m/s; and (**c**) 20 m/s.

Again, this two-phase decomposition was not reflected in the evolution of the static and dynamic porosity ratio, as illustrated in Figure 6.

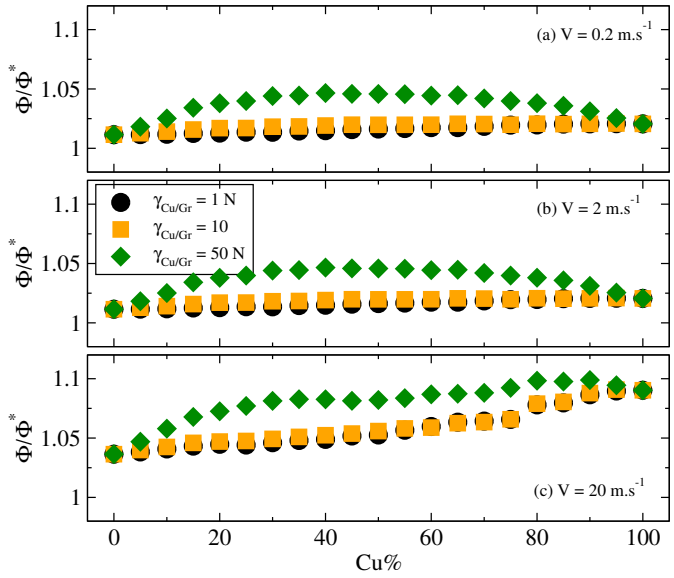

Figure 6. Evolution of the global porosity for different Cu/Gr cohesion (1, 10 and 50 N) and for: (**a**) 0.2 m/s; (**b**) 2 m/s; and (**c**) 20 m/s.

For the highest value of V (i.e., 20 m/s), the evolution was different. As in the case of dry materials, the high shear rate exacerbated the difference between local properties: an almost linear increase of Φ/Φ^* was observed for Cu/Gr cohesion values equal to 1 and 10 N. For the highest cohesion value, Φ/Φ^* increased rapidly with the increase in copper percentage, and then saturated due to the exacerbation of the local copper property by the high shear rate.

Cohesion and shear rate also had a role in the evolution of overall friction (see Figure 7).

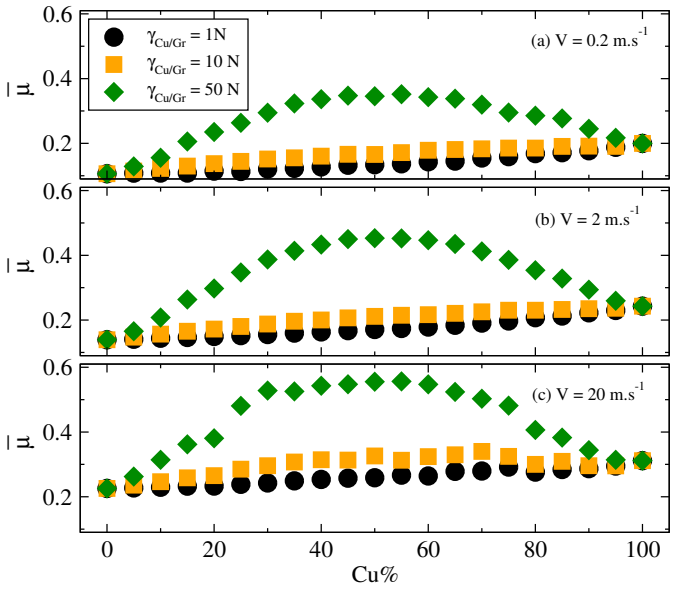

Figure 7. Evolution of the global friction for different Cu/Gr cohesion (1, 10 and 50 N) and for: (**a**) 0.2 m/s; (**b**) 2 m/s; and (**c**) 20 m/s.

For the smallest shear rate values (0.2 and 2 m/s) and for a Cu/Gr cohesion equal to 1 and 10 N, $\bar{\mu}$ increased with the increase in copper percentage: the higher the cohesion or velocity, the higher the friction. For cohesion values equal to 50 N, $\bar{\mu}$ presented a bump-shaped evolution with a maximum value obtained for 50% copper; this maximum value of $\bar{\mu}$ also increased with the shear rate. For the higher shear rate, this dent had a plateau, ranging from 30% to 70% of copper.

3.4. Friction vs. Cohesion

To conclude the investigations on the role of the local properties of copper/graphite mixtures on their global behavior, a final series of simulations was carried out taking into account both friction and cohesion forces. This series was conducted at a speed of 2 m/s, a shear rate that does not exacerbate the local properties of the mixture, thus allowing the competition between friction and cohesion to be analyzed.

With regard to the properties of the mixture, different parameters remained constant during the simulations: Cu/Cu interactions had a friction of 0.6 and a cohesion of 10 N, while Gr/Gr interactions had a friction of 0.05 and a cohesion of 0.01 N. With this set of parameters, a parametric study was performed for different values of Cu/Gr interactions: 0, 0.05 and 0.15 for friction, and 0, 1 and 10 N for cohesion. The same average values as in the previous sections were analyzed.

Figure 8 shows the evolution of the overall electrical resistance for the different friction/cohesion pairs.

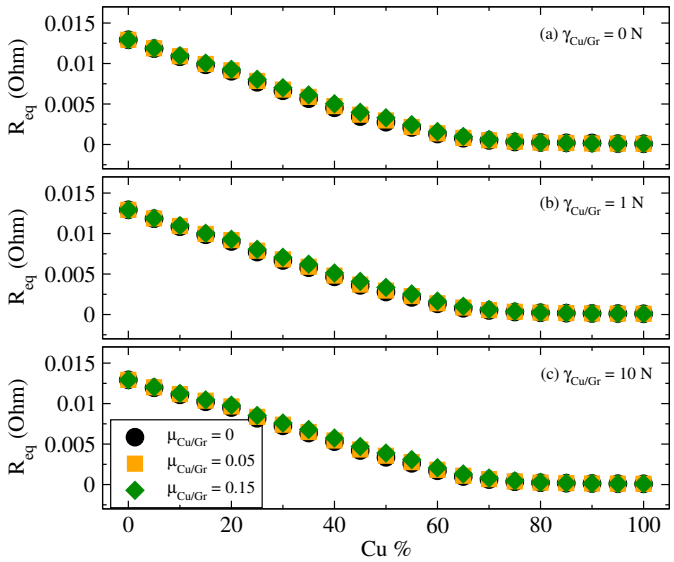

Figure 8. Evolution of the global electrical resistance for different Cu/Gr friction (0, 0.05 and 0.15) and for: (**a**) γ = 0 N; (**b**) γ = 1 N; and (**c**) γ = 10 N.

As observed previously, the resistance R decreased naturally with the proportion of copper, from 10^{-2} Ohm (for 0% Cu) to 10^{-4} Ohm (for 100% Cu) and was independent of the value of the friction Cu/Gr. Within the range of values considered, the differences were negligible. Local properties did not affect macroscopic electrical measurements, which appeared to be more dependent on the applied load.

The effect of local properties combining cohesion and friction was a little more visible on the evolution of the static and dynamic porosity ratio (see Figure 9).

When local cohesion and friction for Cu/Gr interaction were higher, porosity naturally increased with increasing copper percentage. For 50% of copper, the difference between the different friction values increased with increasing cohesion. However, these differences were very small, with the difference between static and dynamic porosities not exceeding 5%.

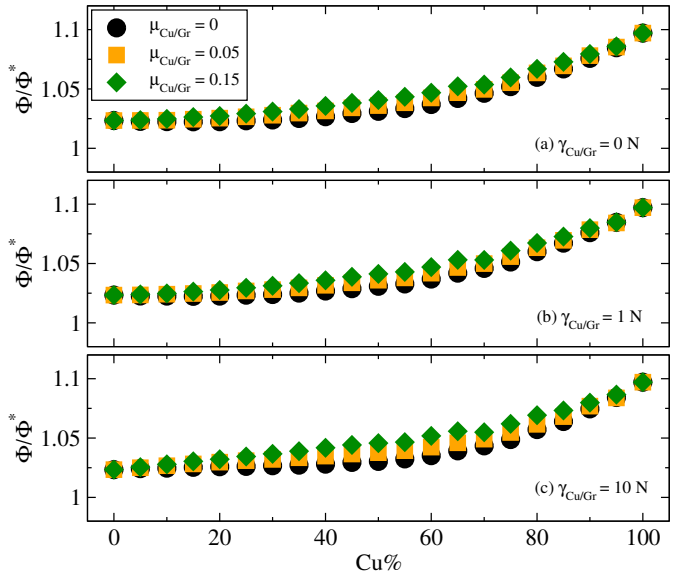

Figure 9. Evolution of the global porosity for different Cu/Gr friction (0, 0.05 and 0.15) and for: (**a**) γ = 0 N; (**b**) γ = 1 N; and (**c**) γ = 10 N.

Finally, the evolution of the overall friction for the different friction and cohesion values Cu/Gr is presented in Figure 10.

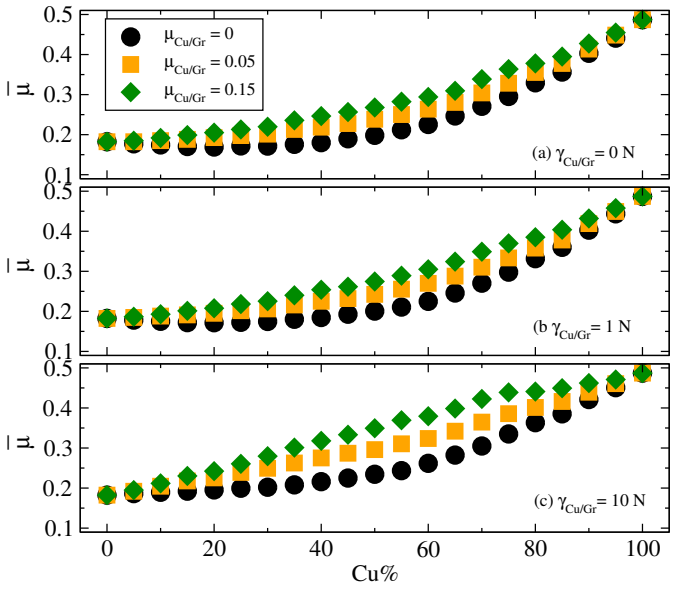

Figure 10. Evolution of the global friction for different Cu/Gr friction (0, 0.05 and 0.15) and for: (**a**) γ = 0 N; (**b**) γ = 1 N; (**c**) γ = 10 N.

The effect of local properties was higher than for porosity or electrical resistance measurements. As with the porosity ratio, $\bar{\mu}$ naturally increased with the increase in copper percentage. When Cu/Gr friction was high, the increase of $\bar{\mu}$ was greater. When the Cu/Gr cohesion increased (in the ranges considered), the evolution of the overall friction was affected in particular for the highest local friction value. When cohesion was equal to 0 or 1 N, the general trend of $\bar{\mu}$ was the same. However, for the strongest cohesion (i.e., 10 N), the curvature of $\bar{\mu}$ changed.

If the Cu/Gr friction was zero, the gradient at the origin was almost zero. When friction increased, the gradient also increased, giving the $\bar{\mu}$ evolution different paces. This underlines the fact that it is important to identify local properties to best describe the interface behavior. Due to the relationship between friction and cohesion, small variations can lead to major differences.

4. Discussion

The various results presented above show that, depending on the global stresses (represented here by different shear rates), the local properties of the mixtures could influence the macroscopic measures.

Before any discussion, it is important to specify that all previous results are correlated to the properties of the material and not to any possible changes in the microstructure of the medium. As shown in Figure 11, which illustrates the final state obtained with samples composed of 50% copper for different shear rates, the shear rate did not affect the distribution of particles in the medium.

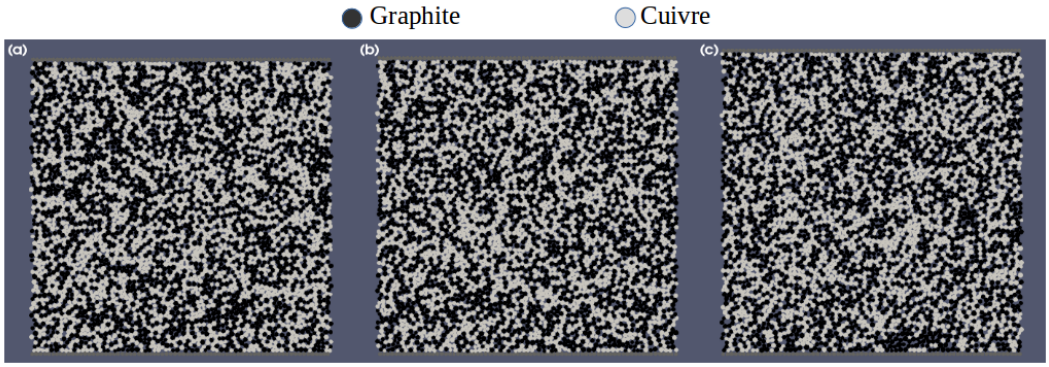

Figure 11. Snapshots of the final state obtained with samples composed of 50% of copper for different shear velocity: (**a**) 0.2 m/s; (**b**) 2 m/s; and (**c**) 20 m/s.

This observation is valid for the different cases previously studied (simulations with or without cohesion, and with or without friction). For example, as shown in Figure 12, there was no variation between the initial and final copper density profile as a function of sample thickness for different shear rates (thickness normalized here by the average diameter).

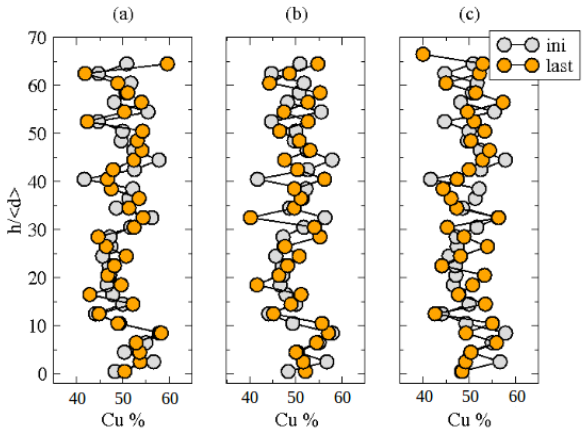

Figure 12. Snapshots of the final state obtained with samples composed of 50% of copper for different shear velocity: (**a**) 0.2 m/s; (**b**) 2 m/s; and (**c**) 20 m/s.

From the measurements presented in the previous sections, several observations can be made. First, the overall electrical resistance did not depend on the local properties of the mixture but on its composition. The evolutions that can occur inside a third body layer seemed to be of a second order with regard to the electrical properties of the different components of the mixture. The transition from linear decay to plateau was only affected by the shear rate, emphasizing once again that global stresses prevail over local properties in terms of electrical resistance.

Secondly, in terms of porosity evolution, the shear rate exacerbated the role of the local properties of the mixture. If for low shear rates, the evolution of porosity seemed to be independent of the copper

percentage, which was no longer the case for a high shear rate. During the mixing of the different components, the high cohesion and friction values did not allow the medium to return to a dense state. However, even if porosities were created locally, it did not affect resistance, probably due to the containment pressure.

Finally, it seemed that the evolution of macroscopic friction was the most dependent on local properties. Depending on the composition of the mixture, the overall friction increased, from a friction value corresponding to pure graphite to a value corresponding to pure copper. This evolution remained very sensitive to the values of interactions between copper and graphite. When these values were equal to zero, the friction evolution was not monotonous with a decrease to a value of 40% of copper and then an increase. Such behavior disappeared with an increase in local cohesion but also with an increase in the shear rate.

In the absence of cohesion (powdery media), the evolution of the overall friction presented a bell whose maximum value was not necessarily reached for a medium composed solely of copper. When the interphase friction was greater than the interphase friction, the maximum value was reached for a copper mixture of 50%.

When considering a cohesive mixture (with or without taking into account the friction between elements), the previous behavior disappeared. The behavior obtained was similar to that observed in the literature [8]. The function corresponding to the results presented in the previous sections was close to a power function (rather than a polynomial of degree 3 or an exponential function [8]). According to local cohesion and friction values, the evolution of the global friction is described by:

$$\bar{\mu} = \mu_* + \alpha x^{\beta}, \tag{6}$$

where α and β are two parameters that depend on the properties of the sample. In a first analysis, it seemed that these two parameters decreased when local cohesion and friction increased (for example, $(\alpha, \beta) = (7 \times 10^{-8}, 3.3)$ when $\mu = 0$ and $\gamma = 0$ and $(\alpha, \beta) = (6 \times 10^{-3}, 0.86)$ when $\mu = 0.15$ and $\gamma = 10$). A more complete parametric study should make it possible to adjust α and β to local parameters.

To complete the discussion, the previous results were compared with the experimental results obtained in the literature. Figure 13 compares the evolution of macroscopic friction presented in Section 3.4 and the work of Su et al. [8] and Kovacik et al. [4].

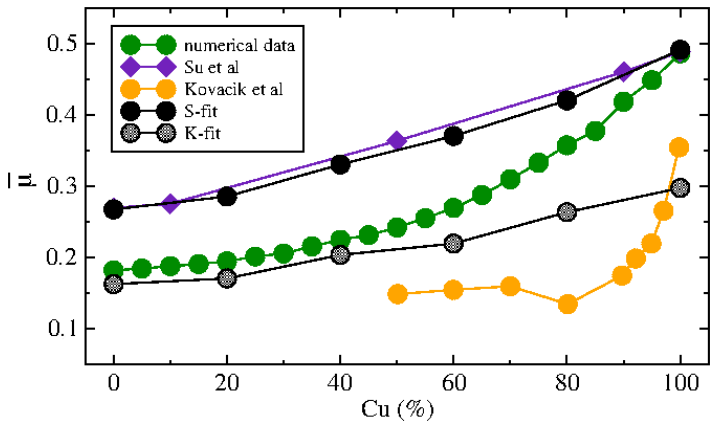

Figure 13. Evolution of the macroscopic friction coefficient for numerical and experimental results for two velocity.

The results of Su et al., Kovacik et al. and those of numerical simulations show an increase in macroscopic friction but with three different evolutions. Concerning the experimental results, this observation is not surprising because the experiments were carried out on materials of a different nature. Indeed, Su et al. [8] studied the influence of a artificial third body made of Cu/Gr powder in a contact between a Cu/Gr composite (60% copper and 15% graphite and additional elements) and a

rotating disc. Kovacik et al. [4] studied the tribological behavior of different Cu/Gr composites with different compositions. Therefore, it is natural for the experimental results to have different curves. As far as numerical simulations are concerned, they are therefore more representative of experimental powder-based work than the latter focused on composites.

However, it can be noted that, for 100% copper, the friction value of the Su et al. results and the numerical results are identical. Thus, to try to match the experimental results obtained by Su et al. [8], a new set of simulations was performed (see S-fit in Figure 13). The values of the Cu/Cu interactions gave a good correspondence, and new cohesion values were given to the Gr/Gr and Gr/Cu interactions (with γ equal to 1 N and 7 N, respectively). The new dataset then shows a perfect match between the experimental results and the numerical results.

Once the model was calibrated (in terms of material properties), the boundary conditions of the Kovacik experimental set-up were applied to the new digital sample and the results obtained are represented in Figure 13 by the $K - fit$ curve. However, there was no correspondence between the experimental results and the numerical results. This is mainly due to the fact that, as mentioned above, the experimental and digital systems were different: a sintered composite and a two-phase powder. However, there were similarities between the two sets of data. Firstly, friction increased with the percentage of copper in the system. Secondly, in both cases, the minimum and maximum friction values were very close.

Finally, it can also be noted that the experimental results show a plateau for copper percentage values below 80%. Therefore, one possible scenario that could explain these differences is as follows. The experimentally generated third body layer did not a priori have the same composition as the sintered material. The latter was probably composed of a higher percentage of graphite, which would tend to delay the results of the experimental curve. Indeed, it should be recalled that the results of Kovacik et al. [4] are represented not in terms of percentage of copper in the third body, but in terms of percentage of copper in the volume. Therefore, it would be interesting to analyze experimental surface states to confirm or refute this scenario in order to complete this study.

5. Conclusions

Numerical studies of a heterogeneous third body layer were carried out and analyzed from a mechanical and electrical point of view. The various results show that the creation of such an interface has a significant impact on its electrical and mechanical properties. In addition, depending on the external stresses (shear rate and containment pressure), different behaviors can be observed. The analysis of the evolution of the global resistance, friction and porosity allows us to understand the influence of the proportion of copper and local parameters. Cohesion influences electrical conduction more than friction; a critical proportion of copper is required to maximize this conduction. It would be interesting to refine the comparison with more experimental results to determine the most favorable local Cu-Gr parameters. Finally, a comparison was made between numerical and experimental results, providing an explanation of the similarities and differences between the experimental results obtained in the literature and the numerical results presented. It underlines the fact that the third body layer may have a completely different behavior and constitution from those of the first bodies and that its characterization remains important for analyzing a tribological problem.

Author Contributions: M.R. and C.Z. developed the numerical method. E.C. developed the interface for the solvers used in the numerical method. E.C. and M.R. performed the simulations, analyzed the data, and wrote the paper with the contribution of Y.B.

Funding: This research received no external funding.

Acknowledgments: The authors wish to thank the developers of the LMGC90 platform who have allowed this investigation.

Conflicts of Interest: The authors declare no conflict of interest.

References

1. Kim, D.H.; Lu, N.; Ma, R. Epidermal Electronics. *Science* **2011**, *333*, 838–843. [CrossRef] [PubMed]
2. Tang, Y.; Liu, H.; Zhao, H.; Liu, L.; Wu, Y. Friction and wear properties of copper matrix composites reinforced with short carbon fibers. *Mater. Des.* **2008**, *29*, 257–261. [CrossRef]
3. Kováčik, J.; Bielek, J. Electrical conductivity of Cu/graphite composite material as a function of structural characteristics. *Scr. Mater.* **1996**, *35*, 151–156. [CrossRef]
4. Kováčik, J.; Emmer, S.; Bielek, J.; Keleši, L. Effect of composition on friction coefficient of Cu-graphite composites. *Wear* **2008**, *265*, 417–421. [CrossRef]
5. Berthier, Y. Experimental evidence for friction and wear modelling. *Wear* **1990**, *139*, 77–92. [CrossRef]
6. Godet, M. The third-body approach: A mechanical view of wear. *Wear* **1984**, *100*, 437–452. [CrossRef]
7. Berthier, Y.; Godet, M.; Brendle, M. Velocity Accommodation in Friction. *Tribol. Trans.* **1989**, *32*, 490–496. [CrossRef]
8. Su, L.; Gao, F.; Han, X.; Fu, R.; Zhang, E. Tribological behavior of copper-graphite powder third body on copper-based friction materials. *Tribol. Lett.* **2015**, *60*, 30. [CrossRef]
9. Su, L.; Gao, F.; Han, X.; Chen, J. Effect of copper powder third body on tribological property of copper-based friction materials. *Tribol. Int.* **2015**, *90*, 420–425. [CrossRef]
10. Su, L.; Gao, F.; Tao, H.; Han, X.; Fu, R. Influence of third body evolution on tribological property of copper-matrix friction material by surface treatment. *AIP Conf. Proc.* **2017**, *1839*, 020001. [CrossRef]
11. Chen, B.; Bi, Q.; Yang, J.; Xia, Y.; Hao, J. Tribological properties of solid lubricants (graphite, h-BN) for Cu-based P/M friction composites. *Tribol. Int.* **2008**, *41*, 1145–1152. [CrossRef]
12. Osterle, W.; Prietzel, C.; Kloß, H.; Dmitriev, A.I. On the role of copper in brake friction materials. *Tribol. Int.* **2010**, *43*, 2317–2326. [CrossRef]
13. Sarnadi, H.; Kokabi, A.H.; Seiyed Reihani, S.M. Friction and wear performance of copper-graphite surface composites fabricated by friction stir processing (FSP). *Wear* **2013**, *304*, 1–12. [CrossRef]
14. Charlery, R.; Renouf, M.; Saulot, A.; Berthier, Y. Experimental and numerical modelling of the ignition of solid propellant. *Tribol. Int.* **2015**, *82*, 330–342. [CrossRef]
15. Radjai, F.; Dubois, F. *Discrete Numerical Modelling of Granular Materials*; ISTE Ltd.: London, UK, 2011; ISBN 978-1-84821-260-2.
16. Renouf, M.; Fillot, N. Coupling electrical and mechanical effect in discrete element simulation. *Int. J. Numer. Meth. Eng.* **2008**, *74*, 238–254. [CrossRef]
17. Zeng, C.; Renouf, M.; Berthier, Y.; Hamdi, R. Numerical investigation on the electrical transmission ability of a shearing powder layer. *Granul. Matter* **2016**, *18*, 19. [CrossRef]
18. Descartes, S.; Renouf, M.; Fillot, N.; Gautier, B.; Descamps, A.; Berthier, Y.; Demanche, P. A new mechanical/electrical approach to the wheel-rail contact. *Wear* **2008**, *265*, 1408–1416. [CrossRef]
19. Elrod, H.G.; Brewe, D.E. Numerical Experiments with Flows of Elongated Granules. In Proceedings of the Lead-Lyon Symposium, Lyon, France, 1991.
20. Iordanoff, I.; Seve, B.; Berthier, Y. Solid Third Body Analysis Using a Discrete Approach: Influence of Adhesion and Particle Size on Macroscopic Properties. *J. Tribol.* **2002**, *124*, 530–538. [CrossRef]
21. Artoni, R.; Santomaso, A.C.; Gabrieli, F.; Tono, D.; Cola, S. Collapse of quasi-two-dimensional wet granular columns. *Phys. Rev. E* **2013**, *87*, 032205. [CrossRef]
22. Azéma, E.; Linero, S.; Estrada, N.; Lizcano, A. Shear strength and microstructure of polydisperse packings: The effect of size span and shape of particle size distribution. *Phys. Rev. E* **2017**, *96*, 022902. [CrossRef] [PubMed]
23. Richard, D.; Iordanoff, I.; Berthier, Y.; Renouf, M.; Fillot, N. Friction Coefficient as a Macroscopic View of Local Dissipation. *J. Tribol.* **2007**, *129*, 829–835. [CrossRef]
24. Renouf, M.; Cao, H.P.; Nhu, V.H. Multiphysical modeling of third body rheology. *Tribol. Int.* **2011**, *44*, 417–425. [CrossRef]
25. Jean, M. The non-smooth contact dynamic method. *Comput. Methods Appl. Mech. Eng.* **1999**, *177*, 235–257. [CrossRef]
26. Maugis, D. Adhesion of spheres–the JKR-DMT transition using a Dugdale model. *J. Colloid Interface Sci.* **1992**, *150*, 243–269. [CrossRef]

27. Renouf, M.; Alart, P. Conjugate gradient type algorithms for frictional multicontact problems: Applications to granular materials. *Comput. Methods Appl. Mech. Eng.* **2004**, *194*, 2019–2041. [CrossRef]
28. Holm, R. *Electrical Contact*; Springer: New York, NY, USA, 1981; ISBN 978-3-662-06688-1.
29. Bowden, F.P.; Tabor, D. *The Friction and Lubrication of Solids*, 2nd ed.; Oxford University Press: Oxford, UK, 1986; ISBN 9780198507772.
30. Greenwood, J.A. Constriction resistance and the real area of contact. *Br. J. Appl. Phys.* **1986**, *17*, 1621–1631. [CrossRef]
31. Da Cruz, F.; Emam, S.; Prochnow, M.; Roux, J.N.; Chevoir, F. Rheophysics of dense granular materials: Discrete simulation of plane shear flows. *Phys. Rev. E* **2005**, *72*, 021309. [CrossRef]
32. Azema, E.; Radjai, F. Internal Structure of Inertial Granular Flows. *Phys. Rev. Lett.* **2014**, *112*, 078001. [CrossRef]
33. Chevoir, F.; Roux, J.N.; Da Cruz, F.; Rognon, P.G.; Koval, G., Jr. Friction law in dense granular flows. *Powder Technol.* **2009**, *190*, 264–268. [CrossRef]